Received: 26 December 2017 | Revised: 29 March 2018 | Accepted: 5 April 2018

DOI: 10.1002/hbm.24192

RESEARCH ARTICLE

WILEY

Fronto-Parietal Subnetworks Flexibility Compensates For Cognitive Decline Due To Mental Fatigue

Fumihiko Taya[1,2] | Stavros I. Dimitriadis[3,4,5] | Andrei Dragomir[2] | Julian Lim[2,6] | Yu Sun[2] | Kian Foong Wong[2] | Nitish V. Thakor[2,7,8,9] | Anastasios Bezerianos[2,10]

[1]Institute of High Performance Computing (IHPC), Agency for Science, Technology and Research (A*STAR), Singapore

[2]Singapore Institute for Neurotechnology (SINAPSE), Centre for Life Sciences, National University of Singapore, Singapore

[3]Institute of Psychological Medicine and Clinical Neurosciences, Cardiff University School of Medicine, Cardiff, United Kingdom

[4]Cardiff University Brain Research Imaging Center (CUBRIC), School of Psychology, Cardiff University, Cardiff, United Kingdom

[5]Neuroinformatics Group, (CUBRIC), School of Psychology, Cardiff University, Cardiff, United Kingdom

[6]Neuroscience and Behavioral Disorders Program, Duke-NUS Graduate Medical School, Singapore

[7]Department of Electrical & Computer Engineering, National University of Singapore, Singapore

[8]Department of Biomedical Engineering, National University of Singapore, Singapore

[9]Department of Biomedical Engineering, Johns Hopkins University, Baltimore, Maryland

[10]School of Medicine, University of Patras, Greece

Correspondence
Anastasios Bezerianos, Singapore Institute for Neurotechnology (SINAPSE), Centre for Life Sciences, National University of Singapore, 28 Medical Drive, #05-Cor, 117456 Singapore.
Email: tassos.bezerianos@nus.edu.sg

Funding information
The National University of Singapore for supporting the Cognitive Engineering Group and Prof. Thakor Startup at the Singapore Institute for Neurotechnology (SINAPSE), Grant/Award Number: WBS R-719-001-102-232 and WBS R-719-000-200-133, respectively; MRC grant, Grant/Award Number: MR/K004360/1 (Behavioural and Neurophysiological Effects of Schizophrenia Risk Genes: A Multi-locus, Pathway Based Approach) (SD); as well as a MARIE-CURIE COFUND EU-UK Research Fellowship

Abstract

Fronto-parietal subnetworks were revealed to compensate for cognitive decline due to mental fatigue by community structure analysis. Here, we investigate changes in topology of subnetworks of resting-state fMRI networks due to mental fatigue induced by prolonged performance of a cognitively demanding task, and their associations with cognitive decline. As it is well established that brain networks have modular organization, community structure analyses can provide valuable information about mesoscale network organization and serve as a bridge between standard fMRI approaches and brain connectomics that quantify the topology of whole brain networks. We developed inter- and intramodule network metrics to quantify topological characteristics of subnetworks, based on our hypothesis that mental fatigue would impact on functional relationships of subnetworks. Functional networks were constructed with wavelet correlation and a data-driven thresholding scheme based on orthogonal minimum spanning trees, which allowed detection of communities with weak connections. A change from pre- to posttask runs was found for the intermodule density between the frontal and the temporal subnetworks. Seven inter- or intramodule network metrics, mostly at the frontal or the parietal subnetworks, showed significant predictive power of individual cognitive decline, while the network metrics for the whole network were less effective in the predictions. Our results suggest that the control-type fronto-parietal networks have a flexible topological architecture to compensate for declining cognitive ability due to mental fatigue. This community structure analysis provides valuable insight into connectivity dynamics under different cognitive states including mental fatigue.

KEYWORDS

community structure analysis, functional brain network, graph theory, intermodule network metrics, intramodule network metrics, modular organization, resting-state fMRI

1 | INTRODUCTION

When continuing to perform a demanding task for an extended period of time, our vigilance level declines, resulting in target detection failure, increased reaction times (RTs) or variability of RTs as well as an increased subjective feeling of fatigue. This effect is known as the "vigilance decrement" or "time-on-task (TOT) effect" (Davies & Parasuraman, 1982; Mackworth, 1948; See, Howe, Warm, & Dember, 1995). A growing body of research has been dedicated to understanding the neural mechanisms underlying mental fatigue and fluctuations in sustained attention with the goal of discovering novel methods to counter its detrimental effects. For example, a study using perfusion fMRI showed that prolonged performance of a taxing cognitive task called the psychomotor vigilance test (PVT) resulted in decreased activity during rest in the attentional fronto-parietal brain area and increased subjective feelings of mental fatigue (Lim et al., 2010). Additionally, many EEG studies have shown that mental fatigue induces changes in θ and α power mainly at frontal and parietal sites respectively, which have been thought to reflect compensatory activity of the attentional network for maintaining performance levels (Barwick, Arnett, & Slobounov, 2012; Bonnefond, Doignon-Camus, Touzalin-Chretien, & Dufour, 2010; Craig, Tran, Wijesuriya, & Nguyen, 2012; Lim, Quevenco, & Kwok, 2013; Tanaka et al., 2012; Trejo, Kubitz, Rosipal, Kochavi, & Montgomery, 2015; Wascher et al., 2014).

As a growing number of studies support the theory that cognitive functions emerge from dynamic interactions among distributed brain areas (Bressler & Menon, 2010), functional connectivity analysis is a useful approach not only for understanding brain functions but also for identifying novel biomarkers of cognitive states. Until now, two methods have generally been used to provide initial insight into brain activity under fatigue: general linear model (GLM)-based univariate approaches of fMRI data and spectral analysis of EEG data. Additionally, several studies of brain networks, including studies by our group, have provided further insight into the neural mechanisms associated with mental fatigue (Breckel et al., 2013; Giessing, Thiel, Alexander-Bloch, Patel, & Bullmore, 2013; Kar, Routray, & Nayak, 2011; Sun et al., 2017; Sun, Lim, Kwok, & Bezerianos, 2014). Exploring network topology based on graph theory is a relatively new approach in the field of brain connectomics (Bullmore & Sporns, 2009; He & Evans, 2010; Sporns, 2013). Based on the connectomics approach, changes in the topological properties of brain functional networks derived from fMRI data associated with vigilance decrements were examined (Breckel et al., 2013; Giessing et al., 2013). Compared to pretask networks, posttask networks demonstrated higher connectivity strength, more clustering, less global efficiency, and shorter distance connections. Additionally, our group has shown changes in one regional property, that is, nodal efficiency, in the resting-state fMRI network (Sun et al., 2017), and also found a decrease in the efficiency of global information transfer in the EEG α band and an asymmetric pattern of connectivity (right $>$ left) in fronto-parietal regions (Sun, Lim, et al., 2014).

In addition, studies of subnetworks can provide further useful information regarding mesoscale network organization (Meunier, Lambiotte, & Bullmore, 2010; Sporns & Betzel, 2016). First, it is well established that the human brain network has a modular organization, consisting of a number of subnetworks dedicated to different perceptual/cognitive functions (Power et al., 2011). Second, community detection is a powerful technique for identifying such subnetworks based on network topology. Therefore, the community structure analysis would be useful for the detection of cognitive states as well as for elucidating the neural underpinnings of cognitive functions. Studies on the modular organization or community structure of brain networks would provide additional information about (1) subnetworks consisting of brain regions dedicated to common cognitive functions, (2) the relationships and communication between such subnetworks, and (3) the topological roles of individual nodes within subnetworks, all of which would be useful for further understanding the neural processes associated with mental fatigue. In fact, modular organization can be altered depending on learning (Bassett et al., 2011), pathological states (Alexander-Bloch et al., 2012; Han et al., 2014; Sun et al., 2014), age (Meunier, Achard, Morcom, & Bullmore, 2009), individual cognitive capacity (Stevens, Tappon, Garg, & Fair, 2012), awareness (Godwin, Barry, & Marois, 2015), and task complexity (Fuertinger & Simonyan, 2016).

In this study, we hypothesize that control-type subnetworks such as the fronto-parietal networks (Zanto & Gazzaley, 2013) would show more flexible topological alterations when mentally fatigued. The fronto-parietal networks were shown to flexibly alter their functional connectivity with other networks depending on requirements by different cognitive tasks (Cole, Smith, & Beckmann, 2013). As such, it is expected that the fronto-parietal networks would also show flexibility to compensate for the declining cognitive functions due to mental fatigue by recruiting other networks more specific to the task, depending on its requirements. To quantify topological characteristics of subnetworks and their inter-relations, we develop metrics specific for the inter- and intramodule connections: the inter- and intramodule density, the inter- and intramodule characteristic path length, and the intramodule clustering coefficient. Subnetworks were identified with a community detection algorithm that partitioned a given network into subnetworks with denser intramodule connections and sparser connections with other subnetworks, and were used for calculating the subnetwork metrics. To induce mental fatigue, participants performed a visual selective attention task inside the scanner, and resting-state fMRI was acquired before and after performing the task. We targeted the short-term effects of prolonged task performance, which were considered to be due to mental fatigue and persisted for at least several minutes (Breckel et al., 2013), rather than long-term training effects. Individual functional networks at pre- and posttask runs were constructed with cutting-edge techniques including maximum overlap discrete wavelet transform (MODWT), Ledoit-Wolf shrinkage covariance estimator (Ledoit & Wolf, 2004) and a data-driven topological filtering scheme based on the orthogonal minimum spanning trees (OMSTs) (Dimitriadis, Antonakakis, Simos, Fletcher, & Papanicolaou, 2017; Dimitriadis, Salis, Tarnanas, & Linden, 2017), which yielded reproducible networks. The subnetwork metrics and conventional metrics for the whole networks were introduced as explanatory variables to regression analyses to examine which metrics were effective in discriminating pre-

and posttask periods and in predicting extents of individual cognitive decline. As the number of explanatory variables was large, a feature selection based on feature importance was performed to reduce the number of features to be included in the regression models. We expected that the network metrics for subnetworks, particularly for the fronto-parietal networks, would show greater predictive power than those for the whole networks.

2 | MATERIALS AND METHODS

2.1 | Participants

Twenty healthy volunteers (12 female, age: 23.1 ± 3.1 years) participated in the study. Participants were students or staff members recruited from the National University of Singapore. All participants gave written consent to take part in the experiment. The study was approved by the NUS institutional ethical review board. The participants completed 2 sessions of fMRI scanning, but only one session is reported in this article. Each participant was paid S$120 in compensation for their effort and time.

All participants were right-handed according to the Edinburgh Handedness Inventory and had normal or corrected-to-normal vision. Additionally, they were pre-screened via a short telephone interview to ensure that they had no history of psychological and physical disorders, no poor eyesight, and no metal implants in their body. Participants were required to have at least eight hours of sleep for the two nights before the experiment and to not consume any caffeine or alcohol for twenty-four hours preceding the study.

2.2 | Experimental design

In this study, we compared the brain functional network during pretask rest with that during posttask rest to investigate changes in the topological architecture of the network, which are associated with TOT effects. Each subject underwent three resting-state runs (R) and four task runs (T) in the order of RTTTTRR (Figure 1a). The task runs were administered between resting-state runs to induce mental fatigue in participants. In the resting-state runs, a white fixation cross was presented in the center of the screen while the subject was lying calmly at rest with eyes open. In the task runs, subjects performed a visual oddball task mentioned below. The duration of each run was 5 min and 26 s, including the fixation cross presentation for 6 s preceding the task and an extra fixation cross presentation for 20 s following the task. In this study, the resting-state data at the first (Rest1) and sixth (Rest2) run were used for further analysis to compare the modular organization of the intrinsic functional network during pretask rest with that during posttask rest.

2.3 | Behavioral task and questionnaire

A visual oddball task was used as the selective attention task to induce TOT effects inside the MRI scanner (Figure 1b). In the visual oddball task, participants were required to press a button when the target letter (selected from a group of four alphabet letters 'b','d','p' and 'q') was

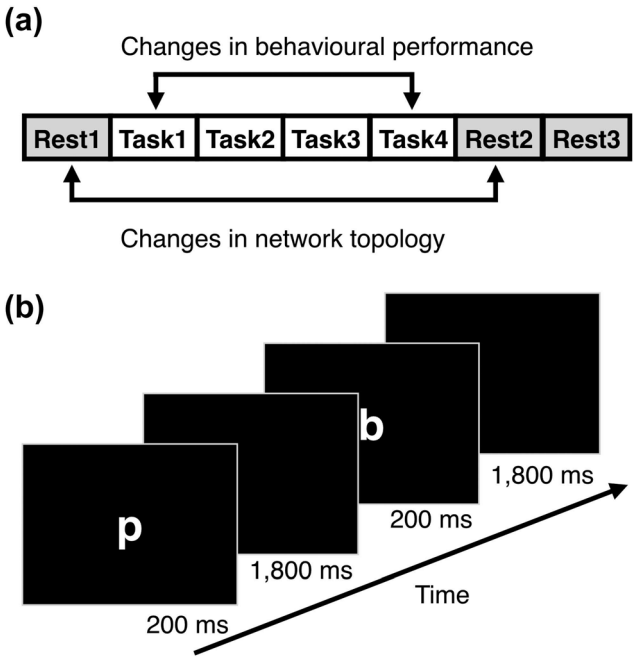

FIGURE 1 Experimental design. Each participant underwent three rest (R) and four task (T) runs in the order of RTTTTRR (a). Changes in the network metrics of each subnetwork were examined for Rest1 vs. Rest2. Additionally, the correlation between changes in median RT (linear trends of changes in RT from Task1 to Task4) and changes in network topology of subnetworks (Rest2 - Rest1) was investigated. During the rest runs, a white fixation cross was presented at the center of the screen, and the participant laid calmly on his or her back with eyes open. During the task runs, the participant performed a visual oddball task, in which four alphabet characters ('b', 'd', 'p' and 'q') were presented in a random order, and the participant was instructed to press the button when the pre-defined target letter was presented (b). The target was different for each run. Each run consisted of 150 trials: 30 target, 90 non-target, and 30 null trials. The duration of each run was 5 min and 26 s

presented at the center of the screen while these four letters were continually alternated in a random order in the center of the screen. Each run consisted of 150 trials: 30 target, 90 non-target, and 30 null trials. The target letter was different for each run. For each trial, the character was presented for 0.2 s, followed by presentation of the fixation cross for 1.8 s. The trial sequences were generated using optseq (http://surfer.nmr.mgh.harvard.edu/optseq). Participants were instructed to respond as quickly as possible to a target while maintaining a low error rate.

We examined the hit rates and RT for correct responses as measures of the overall level of performance. To assess the TOT effect, we obtained the median RT and the mean hit rates for each participant and conducted one-way repeated-measures analysis of variance (ANOVA) on these factors with runs as an independent variable.

Before and after the MRI session, each participant completed the Short Stress State Questionnaire (SSSQ) outside the scanner to assess subjective feelings of mental fatigue (Helton, 2004). The twenty-four SSSQ items were divided into three scales: Engagement, Distress and

Worry. SSSQ scores were averaged across each scale and were subjected to paired *t*-tests to compare subjective feelings of stress at pre- and posttask. We expected that task engagement would decrease as typically observed in tests of vigilance (Matthews, Szalma, Panganiban, Neubauer, & Warm, 2013).

Stimuli were presented using Psychtoolbox (Brainard, 1997; Pelli, 1997) on a NordicNeuroLab LCD Monitor 32" (NordicNeuroLab Inc., Norway, www.nordicneurolab.com) behind the scanner, viewed through a mirror placed on the head coil. Behavioral responses during the MRI scan were collected using a Current Designs HHSC-2x4-C (Current Designs, Inc., Philadelphia, www.curdes.com) response pad through a Current Designs fORP 932 electronic interface. The statistical tests of the behavioral and questionnaire data were performed using MATLAB (Mathworks, USA).

2.4 | fMRI data acquisition

fMRI scanning took place at the A*STAR-NUS Clinical Imaging Research Centre (CIRC) in the medical school of the National University of Singapore. Echo planar imaging (EPI) data were acquired using a Siemens 3T Prisma scanner (Siemens, Erlangen, Germany). Thirty-three axial slices parallel to the AC-PC plane were collected with the following parameters in an interleaved order: slice thickness = 3.5 mm; inter-slice gap = 0.70 mm; matrix size = 74 × 74; flip angle = 90°; TR = 2,000 ms; TE = 30 ms; in-plane resolution = 3.0 mm; FOV = 220 mm. Seven runs of fMRI data acquisition lasting for 5 min and 26 s (163 volumes) were performed for each participant. A high resolution (1.0 × 1.0 × 1.0 mm^3) sagittal T1-weighted MP-RAGE (TR = 2,000 ms; TE = 2.45 ms; FOV = 250 mm; flip angle = 8°) was acquired to facilitate registration and normalization of functional data.

2.5 | fMRI data preprocessing

fMRI data were preprocessed using the FMRIB Software Library (FSL) analysis package (Jenkinson, Beckmann, Behrens, Woolrich, & Smith, 2012). Preprocessing steps comprised head motion correction, slice timing correction, spatial smoothing with a Gaussian kernel of FWHM 6 mm, grand-mean intensity normalization, and high-pass temporal filtering with $\sigma = 50$ s. Exclusion criteria of head motion exceeding 3 mm in translation or 3° in rotation were regarded as excessive; however, no data met these criteria. The high-resolution T1-weighted images were registered to the MNI standard space to normalize individual data to the standard space. Cerebral spinal fluid (CSF) and white matter were then segmented from individual structural images, registered to the standard space, co-registered to individual functional space, and used for extracting the average CSF signal and the average white matter signal. The six parameters from motion correction and the average CSF and white matter signals were introduced as nuisance parameters into the general linear model (GLM). The global signal was not included as a nuisance parameter in the regression as it would introduce anti-correlated structure into the functional network (Murphy, Birn, Handwerker, Jones, & Bandettini, 2009). The residuals after the regression were co-registered with the MNI standard space and were used for the further analysis. To ensure that differences found in fMRI data were not attributed to head motion, we examined frame-wise displacement (FD) (Power, Barnes, Snyder, Schlaggar, & Petersen, 2012). Average FDs were small (mean ± SD, pretask: 0.08 ± 0.04 mm, posttask: 0.09 ± 0.06 mm), and a paired *t*-test revealed no significant difference between the pre- and posttask resting periods ($t_{19} = 1.62$, $p = 0.12$).

2.6 | Network construction

To examine alterations in the network topology of brain subnetworks due to mental fatigue, we constructed functional connectivity maps based on wavelet correlation matrices. First, time series of BOLD signals were extracted from the functional data normalized to the standard brain for 112 regions of interest (ROIs) based on the Harvard-Oxford cortical and subcortical atlases (Kennedy et al., 1998; Makris et al., 1999), which is a good compromise in terms of spatial resolution, computational costs and the performance in community detection (Taya, de Souza, Thakor, & Bezerianos, 2016), and averaged over voxels within each ROI, resulting in 112 sets of time-series data. To construct functional networks, inter-regional correlation coefficients (Lindsay, Percival, & Rothrock, 1996; Whitcher, Guttorp, & Percival, 2000) were estimated with the Ledoit-Wolf shrinkage covariance estimator (Ledoit & Wolf, 2004) on wavelet coefficients decomposed with the maximal overlap discrete wavelet transform (MODWT) in five wavelet scales. Daubechies least asymmetric wavelet filter with a wave length of 8 was used (Zhang, Telesford, Giusti, Lim, & Bassett, 2016). In this study, we focused on the scale of 2, which corresponds to the frequency range of 0.06 - 0.125 Hz. The absolute values of Fisher's Z-transformed correlation coefficients were then thresholded with the data-driven topological filtering scheme based on optimization of the global cost-efficiency of the network (Bassett et al., 2009) and the OMSTs (Dimitriadis, Antonakakis, et al., 2017; Dimitriadis, Salis, et al., 2017) (see Appendix A for more details). The obtained topological undirected weighted graphs were used for the subsequent community structure analysis.

PyWavelets (https://pywavelets.readthedocs.io/), scikit-learn (Pedregosa et al., 2011) packages and in-house Python scripts were used for network construction, Nilearn (http://nilearn.github.io/) and BrainNet Viewer on MATLAB (Xia et al., 2013) were used to visualize brain atlases, and python-igraph (http://igraph.org/python/) was used to visualize topological graphs. A flowchart of the individual network construction is presented in Figure 2.

2.7 | Brain subnetworks

The brain network is known to consist of subnetworks that are involved in different cognitive functions. To explore the topological characteristics of such subnetworks, a community detection algorithm was applied to the obtained functional connectivity patterns.

In graph theory, such subnetworks are usually called communities or modules. Communities are generally defined as subgroups of nodes in a network, which are densely interconnected with each other (Newman & Girvan, 2004; Radicchi, Castellano, Cecconi, Loreto, & Parisi,

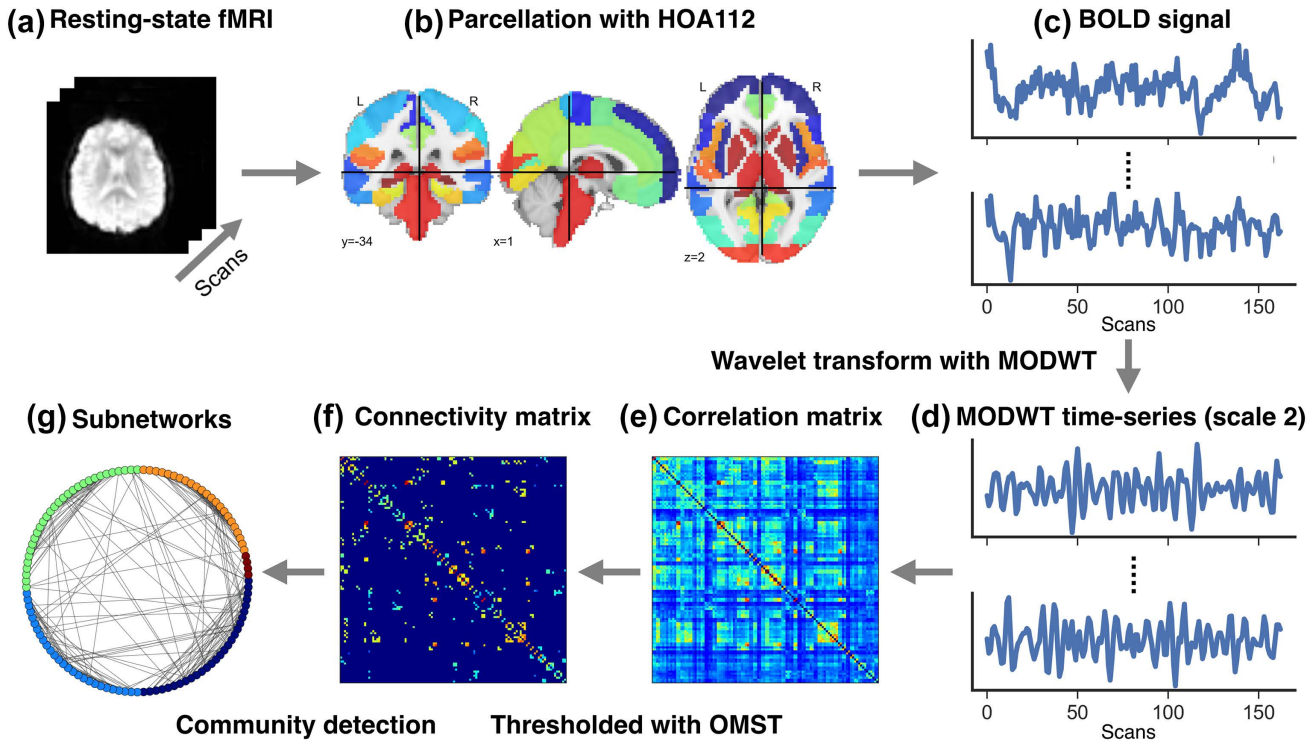

FIGURE 2 Flowchart of the construction of individual networks and modular decomposition. For each participant and each run, resting-state BOLD fMRI data were acquired (a) and pre-processed. The pre-processed signals were parcellated according to the Harvard-Oxford atlas (HOA) (b) to derive 112 BOLD time-series data averaged over voxels within each brain region (c). The averaged BOLD signals were decomposed with the maximal overlap discrete wavelet transform (MOWDT) (d). In this study, we focused on the wavelet scale of 2, which corresponded to the frequency range of 0.06 to 0.125 Hz. Next, a wavelet correlation matrix was obtained with the Ledoit-Wolf shrinkage covariance estimator of the power of the wavelet coefficients (e). The Fisher's Z-transformed correlation matrix was thresholded with the data-driven topological filtering scheme based on the orthogonal minimum spanning trees (OMSTs), yielding a topological graph (f). The graph was decomposed into subnetworks via the Louvain method for community detection, according to the protocol introduced by Sporns and Betzel (Sporns & Betzel, 2016) (g)

2004). To decompose networks into communities, several algorithms have been proposed (Fortunato, 2010; Newman, 2012). In this study, the Louvain algorithm, a fast and relatively accurate algorithm for finding a community structure that maximizes modularity (see Appendix B), was applied to the derived functional networks for modular decomposition (Blondel, Guillaume, Lambiotte, & Lefebvre, 2008). Additionally, we followed the protocol introduced by Sporns and Betzel (Sporns & Betzel, 2016) to optimize hyper-parameters and to overcome the heuristic nature of the community detection algorithm.

Furthermore, it is important to find a consensus community structure that is representative of the entire group of participants to discuss the roles of brain subnetworks in different conditions on common ground (Taya et al., 2016). To obtain such a representative set of subnetworks, individual community structures were first detected for the resting-state functional networks at Rest1, and a consensus community structure was obtained with a consensus clustering algorithm (Bassett et al., 2013; Lancichinetti & Fortunato, 2012). The derived representative community structure was used to calculate the network metrics of the subnetworks described below.

First, individual community structures were obtained in the following manner. For each individual network, the resolution parameter γ, which maximizes the difference in modularity between the empirical network and the average of 100 randomized networks, was selected to obtain a community structure for each individual network, following the protocol introduced by Sporns and Betzel (Sporns & Betzel, 2016). The results of modular decomposition can vary every time the algorithm is executed due to its heuristic nature, even though the variation in modularity over the execution is negligible (Blondel et al., 2008). Therefore, modular decomposition was performed 100 times for the selected spatial resolution parameter to yield an association matrix representing how many times each node pair was assigned to the same community. The empirical association matrix was then thresholded with the maximum value of association matrices of null partition matrices generated randomly 100 times by permuting the empirical association matrix, and consensus clustering was performed to obtain a consensus partition. The obtained consensus partition was regarded as the individual community structure. Finally, the resultant twenty individual community structures were used to find a representative community structure with the consensus clustering.

A brain connectivity package on Python (Rubinov & Sporns, 2010) and in-house scripts in Python were used for the identification of subnetworks.

2.8 | Topological characteristics of mesoscale networks

To investigate changes in the topological characteristics of intermediate-scale of the functional brain network induced by performing the intense attentional task, we define the following network metrics for inter- and intramodule connections by adapting network metrics defined for large-scale networks (Rubinov & Sporns, 2010; Watts & Strogatz, 1998) to subnetworks.

The intramodule density d_u of module u is defined as the proportion of actual connections between nodes in the module u to potential connections,

$$d_u = \frac{1}{N_u(N_u-1)} \sum_{i,j\in u, j\neq i} a_{ij}$$

where a_{ij} is an element of an adjacency matrix, which is 1 if there is an edge between node i and j, and is 0 otherwise, and N_u is the size of the module u. Thus, the intramodule density d_u is the density of the network, which consists of nodes within the module u and edges between the nodes.

The intermodule density d_{uv} of inter-connections between modules u and v is defined as the proportion of actual connections between the nodes in the module u and the nodes in the module v to potential connections,

$$d_{uv} = \frac{1}{N_u N_v} \sum_{i\in u} \sum_{j\in v} a_{ij}$$

where a_{ij} indicates whether there is an edge between node i in the module u and node j in the module v. N_u and N_v are the size of the module u and that of the module v, respectively. Higher intermodule density indicates that connections between the modules are denser.

The intramodule characteristic path length L_u is defined as follows,

$$L_u = \frac{1}{N_u(N_u-1)} \sum_{i,j\in u, j\neq i} l_{ij}$$

where l_{ij} is the shortest path length between node i and j. Thus, the intramodule characteristic path length L_u is the characteristic path length of the network, which consists of nodes within the module u and edges between the nodes. Shorter intramodule characteristic path length indicates higher efficiency in communications within the module.

The intermodule characteristic path length L_{uv} is defined as follows,

$$L_{uv} = \frac{1}{N_u} \sum_{i\in u} \frac{1}{N_v} \sum_{j\in v} l_{ij}$$

where l_{ij} is the shortest path length between node i in the module u and node j in the module v. Shorter intermodule characteristic path length indicates higher efficiency in communications between the modules.

The intramodule clustering coefficient C_u is defined as follows,

$$C_u = \frac{1}{N_u} \sum_{i\in u} \frac{\sum_{j,k\in u} (w_{ij} w_{jk} w_{ki})^{1/3}}{k_i(k_i-1)}$$

where w_{ij} is weights of connections between node i and j, and k_i is the degree of node i. The intramodule clustering coefficient C_u is the clustering coefficient of the subnetwork.

The network metrics regarding inter- and intramodule connections defined above, that is, the inter- and the intramodule density, the inter- and the intramodule characteristic path length and the intramodule clustering coefficient were calculated using the obtained representative community structure of the individual connection matrices. Furthermore, network metrics for global characteristics of large-scale of networks, that is, the density d, the characteristic path length L and the clustering coefficient C of the whole networks, were calculated (Rubinov & Sporns, 2010; Watts & Strogatz, 1998). In-house scripts in Python and the brain connectivity package in Python were used to calculate the network metrics.

2.9 | Regression analyses on network metrics

To examine the effects of intense task performance on the topological characteristics of the subnetworks of the functional brain network, regression analyses were performed on the network metrics. We first performed a logistic regression analysis with Run as response variable and network metrics as explanatory variables to explore what characteristics of the network topology predict difference between pre- and posttask runs, that is, Rest1 vs. Rest2. The difference in the density of the whole network at Rest1 and Rest2 was also examined with a nonparametric permutation test with 10,000 resamples using the adjusted P value (North, Curtis, & Sham, 2002; Sham & Purcell, 2014). Furthermore, as there were large individual differences in the extent of the cognitive decline induced by the task performance, we further investigated the correlation of changes in network metrics (Rest2 - Rest1) with the observed cognitive decline measured with the changes in median RT (individual linear trends of the changes in RT from Task1 to Task4). To investigate which network characteristics were associated with the cognitive decline, we performed a multivariate linear regression analysis, in which the linear trend in RT is a response variable and network metrics are explanatory variables. The individual linear trends in RT were standarized with its mean and SD. The change in the subjective feeling of fatigue measured with the Engagement scale of the SSSQ questionnaire was also examined, while the change in the hit rate was not examined due to its small variability among participants.

2.10 | Feature selection for the regression models

As the number of explanatory variables was large, a feature selection based on feature importance was performed using the ridge regression with the cross-validation technique. The ridge regularization, also called L_2 regularization, is a method of regularization of ill-posed problems, which shrinks the coefficient estimates towards zero by introducing a shrinkage penalty term into the objective function (Hastie, Tibshirani, & Friedman, 2009). The tuning parameter λ of the ridge regularization was optimized with the generalized cross-validation, and the importance weights of the features were calculated with the optimized λ for the feature selection. Please note that the regularization was applied only for the feature selection.

The number of metrics for intermodule connections is ${}_N C_2$, where N is the number of modules, for each kind of metric. Although the

TABLE I Twenty-seven network metrics introduced into the feature selection and the regression analyses, including three metrics for the whole network, 12 intramodule metrics and twelve intermodule metrics

			Rest1 vs. Rest2		Correlation with RT changes	
			p-value	β	*p*-value	β
whole network	Density	d	$p^* = 0.015$	-	-	-
	Characteristic path length	L	-	-	-	-
	Clustering coefficient	C	-	-	-	-
Intramodule metrics	Density d_u	d_F	-	-	0.0006	−0.6
		d_P	-	-	-	-
		d_T	-	-	-	-
		d_O	-	-	-	-
	Characteristic path length L_u	L_F	-	-	-	-
		L_P	-	-	0.0001	−0.89
		L_T	-	-	-	-
		L_O	-	-	-	-
	Clustering path length C_u	C_F	-	-	-	-
		C_P	-	-	0.03	0.36
		C_T	-	-	-	-
		C_O	-	-	-	-
Intermodule metrics	Density d_{uv}	d_{FP}	-	-	-	-
		d_{FT}	0.017	1.05	-	-
		d_{FO}	-	-	-	-
		d_{PT}	-	-	0.0006	0.62
		d_{PO}	-	-	-	-
		d_{TO}	-	-	0.02	0.31
	Characteristic path length L_{uv}	L_{FP}	-	-	-	-
		L_{FT}	-	-	0.00002	1.31
		L_{FO}	-	-	-	-
		L_{PT}	-	-	-	-
		L_{PO}	-	-	0.004	−0.42
		L_{TO}	-	-	-	-

The subscripts indicate the four subnetworks: frontal *F*, parietal *P*, temporal *T* and occipital *O* subnetworks. The subcortical *S* subnetwork was not examined due to its small size. For the intermodule metrics, the metrics were calculated for all possible six intermodule connections. The *p*-values and coefficient values are the results of the logistic regression for Rest1 vs. Rest2 comparison and those of the multivariate linear regression analysis for the correlation with the linear trends in median RT during the task runs, except the p^*-value for the density of the whole network obtained with the permutation test to compare Rest1 and Rest2. The hyphen "-" indicates the features, which were not selected with the feature selection

number of identified subnetworks was five, metrics for the subcortical subnetwork were not used because of its small size. Thus, the other four subnetworks were examined. Consequently, the total number of explanatory variables was twenty-seven, including twelve variables for the intermodule connections, twelve for the intramodule metrics and three metrics for the whole networks (see Table I).

For the difference between Rest1 and Rest2, only one explanatory variable, the intermodule density between the frontal and the temporal subnetworks d_{FT}, was selected with the ridge classifier and 4-folds cross-validation. A logistic regression analysis was performed with the selected feature to see whether the effect of the feature was significant for discriminating Rest1 and Rest2.

For the correlation with cognitive decline measured with the changes in median RT, the explanatory variables were reduced to seven features, including the intermodule density between the parietal and the temporal subnetworks d_{PT}, that between the temporal and the occipital subnetworks d_{TO}, the intermodule characteristic path length between the frontal and the temporal subnetworks L_{FT}, that between

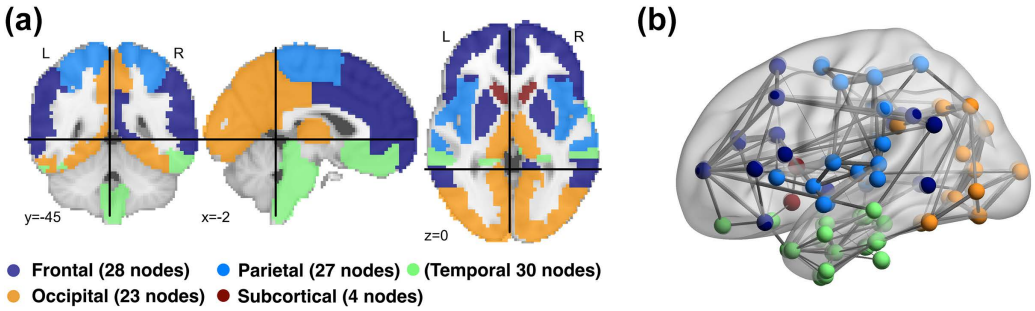

FIGURE 3 The representative community structure of individuals obtained with consensus clustering. The resultant community structure consisted of five subnetworks: frontal, parietal, temporal, occipital and subcortical subnetworks (a), which were generally consistent with previous studies showing modular organization of functional brain networks. The representative community structure obtained at pretask run (Rest1) and the average connectivity at Rest1 overlaid on an image of the brain surface is depicted in (b)

the parietal and the occipital subnetworks L_{PO}, the intramodule density of the frontal subnetwork d_F, the intramodule characteristic path length of the parietal subnetwork L_P, and the intramodule clustering coefficient of the parietal subnetwork C_P, with the ridge regression and 4-folds cross-validation. No metrics for the whole network were selected. The selected seven features were introduced to a multivariate linear regression model to examine whether the features were significantly effective for predicting the individual changes in RT. For the changes in the Engagement scale of the SSSQ questionnaire, no features were selected.

Scikit-learn and StatsModels (http://www.statsmodels.org/) packages in Python were used for the feature selection and the regression analyses, in addition to in-house scripts in Python. The significance level of 0.05 was used.

3 | RESULTS

3.1 | Behavioral results

To ensure that the attentional task induced the TOT effect, we examined changes in the median RT and hit rates over the four task runs while the participants were performing the visual oddball task. The mean hit rate was 93.7% ($SD = 6.4$), and the average median RT over all participants was 583.5 msec ($SD = 50.3$). Performing the visual oddball task elicited a clear TOT effect as revealed by an increase in the RT and a decrease in the hit rate over the course of the runs, as shown in Figure 4. One-way repeated-measures ANOVA on the median RTs and the hit rates with the runs as an independent variable revealed a significant effect of TOT (hit rate: $F_{3,57} = 2.86$, $p = 0.045$, RT: $F_{3,57} = 3.32$, $p = 0.026$).

We also examined changes in the subjective feeling of mental fatigue assessed via SSSQ scores. The average SSSQ scores for the Engagement scale were 3.66 ($SD = 0.57$) at pretask and 3.19 ($SD = 0.73$) at posttask, those for the Distress scale were 1.29 ($SD = 0.57$) at pretask and 1.28 ($SD = 0.40$) at posttask, and those for the Worry scale were 2.49 ($SD = 0.92$) at pretask and 2.48 ($SD = 1.06$) at posttask. As expected, separate paired t-tests showed a significant decrease in the Engagement scale ($t_{19} = 3.27$, $p = 0.04$) while no significant differences were found for the Distress ($t_{19} = 0.23$, $p = 0.82$) and Worry ($t_{19} = 0.10$, $p = 0.92$) scales. Of note, the SSSQ was administered after participants got out of the MRI scanner, revealing that the decrease in subjective scores of the Engagement scale was observed even after the participants were allowed a break during the two resting-state and structural runs, which was typically over 20 min from completion of the task performance.

Taken together, the behavioral measures and the subjective scores revealed that the visual oddball task induced TOT effects, consistent with previous studies that have shown robust associations with genetic and physiological markers of TOT (Lim et al., 2012; Lim et al., 2013; Lim et al., 2010).

3.2 | Subnetworks of the functional network

Consensus community detection identified five subnetworks in the representative community structure for the whole group of participants, as shown in Figure 3. The average modularity Q across individual networks was 0.40 ($SD = 0.06$) at Rest1 and 0.38 ($SD = 0.06$) at Rest2, both of which were regarded to be modular (Newman & Girvan, 2004). The numbers of brain areas assigned to the subnetworks ranged from 4 to 30. As shown in Figure 3, the five subnetworks consisted of brain areas in the frontal lobe extending to the parietal lobe and the limbic system (blue), the parietal lobe (sky blue), the temporal lobe (green), the occipital lobe extending to the thalamus (orange), and the subcortical areas (brown), which were generally consistent with previous studies showing modular organization of functional brain networks (Cole et al., 2010; Crossley et al., 2013; He et al., 2009; Meunier, Achard, et al., 2009; Meunier, Lambiotte, Fornito, Ersche, & Bullmore, 2009; Power et al., 2011; Yeo et al., 2011).

3.3 | Changes in the topological characteristics of subnetworks

When comparing the averaged connection matrices across participants at pre- with those at posttask (Figure 5a), the averaged networks are visually denser at posttask. Please note that these average graphs were obtained only for demonstration purpose, with the protocol on the average correlation matrices across participants, the same as the individual connection matrices, and were not used for the data analysis. As

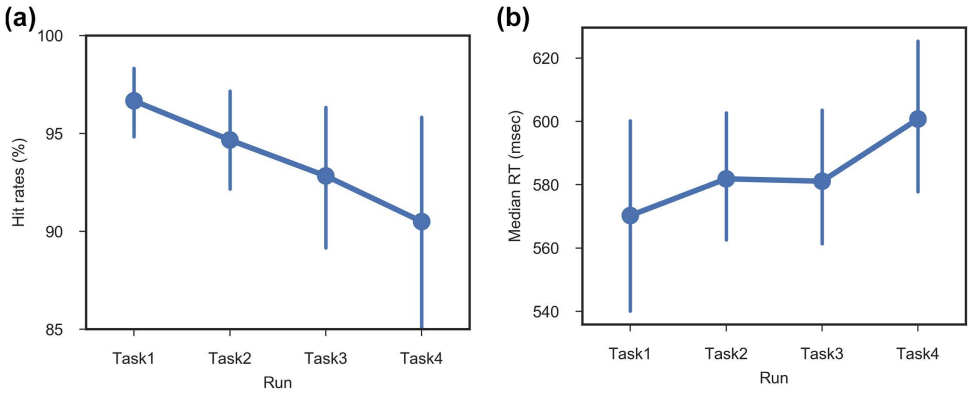

FIGURE 4 Changes in hit rates (a) and median RTs (b) over the four task runs. A significant effect of time-on-task was observed, which was manifested as a decrease in hit rates and an increase in median RTs. Error bars indicate 95% confidence intervals estimated with bootstrapping [Color figure can be viewed at wileyonlinelibrary.com]

hypothesized, changes in intermodule network topology were observed at the fronto-parietal networks. The circular representations of the networks showed denser intermodule connections particularly for connections between the frontal and the temporal subnetworks at posttask compared to pretask (Figure 5b). As can be seen in Figure 5a, the OMSTs-based topological filtering produced topological graphs, in which weak connections were kept particularly in the temporal subnetwork.

The observation was confirmed with statistical tests on global characteristics of the network (Figure 6). First, the density level of the whole network averaged across the individual networks was 0.054 ($SD = 0.016$) at Rest1 and 0.065 ($SD = 0.014$) at Rest2 respectively (Figure 6a). Significant differences were found for Rest1 vs. Rest2 ($p^* = 0.015$). The increase in the density of the whole network may be attributable to an increased density in the intermodule connections between the frontal and the temporal networks as observed in the averaged networks (Figure 5b). The logistic regression analysis showed that the effect of d_{FT} was significant ($\beta = 1.05$, $p = 0.017$, 95% CI [0.19, 1.91]) for discriminating Rest1 and Rest2 as shown in Figure 6b. The model predicted 65.0% of the responses correctly. The McFadden's R^2 was 0.14.

Although we found a significant difference between the pre- and posttask periods, such a difference could be attributed to mental habituation to the scanning environment. Additionally, there were individual differences in TOT effects, which may obscure the effects of metal fatigue and compensatory activity. Therefore, we conducted a multivariate linear regression analysis on the relationship between changes in the network metrics and the observed cognitive decline. The results of the regression indicated that the seven features explained 88.5% of the variance (*adjusted* $R^2 = 0.885$, $F_{7,13} = 23.06$, $p = 0.000002$). All seven features selected with the feature selection showed significant effects (Table I). The changes in the intermodule network metrics including d_{PT} ($\beta = 0.62$, $p = 0.0006$, 95% CI [0.32, 0.91]), d_{TO} ($\beta = 0.31$, $p = 0.02$, 95% CI [0.07, 0.56]) and L_{FT} ($\beta = 1.31$, $p = 0.00002$, 95% CI [0.88, 1.73]) showed positive effects, while the change in L_{PO} ($\beta = -0.42$, $p = 0.004$, 95% CI [-0.68, −0.16]) showed a negative effect on the prediction of the change in RT. Furthermore, an intramodule network metric C_p ($\beta = 0.36$, $p = 0.03$, 95% CI [0.05, 0.66]) showed a positive effect, while the other two intramodule metrics showed negative effects: d_F ($\beta = -0.60$, $p = 0.0006$, 95% CI [-0.88, −0.31]) and L_p ($\beta = -0.89$, $p = 0.0001$, 95% CI [-1.25, −0.53]). Figure 7 shows the partial regression plots for the intermodule metrics, while Figure 8 shows those for the intramodule metrics.

We aimed to investigate whether the observed changes were associated with mental fatigue and whether they were localized to specific subnetworks such as the control-type frontal and parietal networks. As hypothesized, most of the network metrics showing significant predictive power were found at the flexible control-type fronto-parietal subnetworks.

4 | DISCUSSION

In this study, we investigated the effects of mental fatigue on the topological characteristics of brain functional subnetworks, which were obtained with a community detection technique based on graph theory. Using the representative community structure of the network, we investigated changes in the topological characteristics of subnetworks induced by prolonged performance of an attention task and their associations with changes in behavioral performance. To this end, we developed the inter- and intramodule metrics, that is, the inter- and the intramodule density, the inter- and the intramodule characteristic path length and the intramodule clustering coefficient, by adapting the metrics for large-scale networks to the intermediate-scale of networks. Interestingly, although the network metrics for the whole network were also examined, no such metrics were selected with the feature selection, suggesting that the inter- and the intramodule network metrics were more pronounced in capturing the topological characteristics of the network associated with the cognitive decline due to the task performance. Furthermore, the changes in network topology from pre- to posttask periods were also more pronounced in the intermediate-scale of networks, compared to the whole network. Taken together, newly developed metrics for the inter- and the intramodule connections revealed greater predictive powers in both the associated

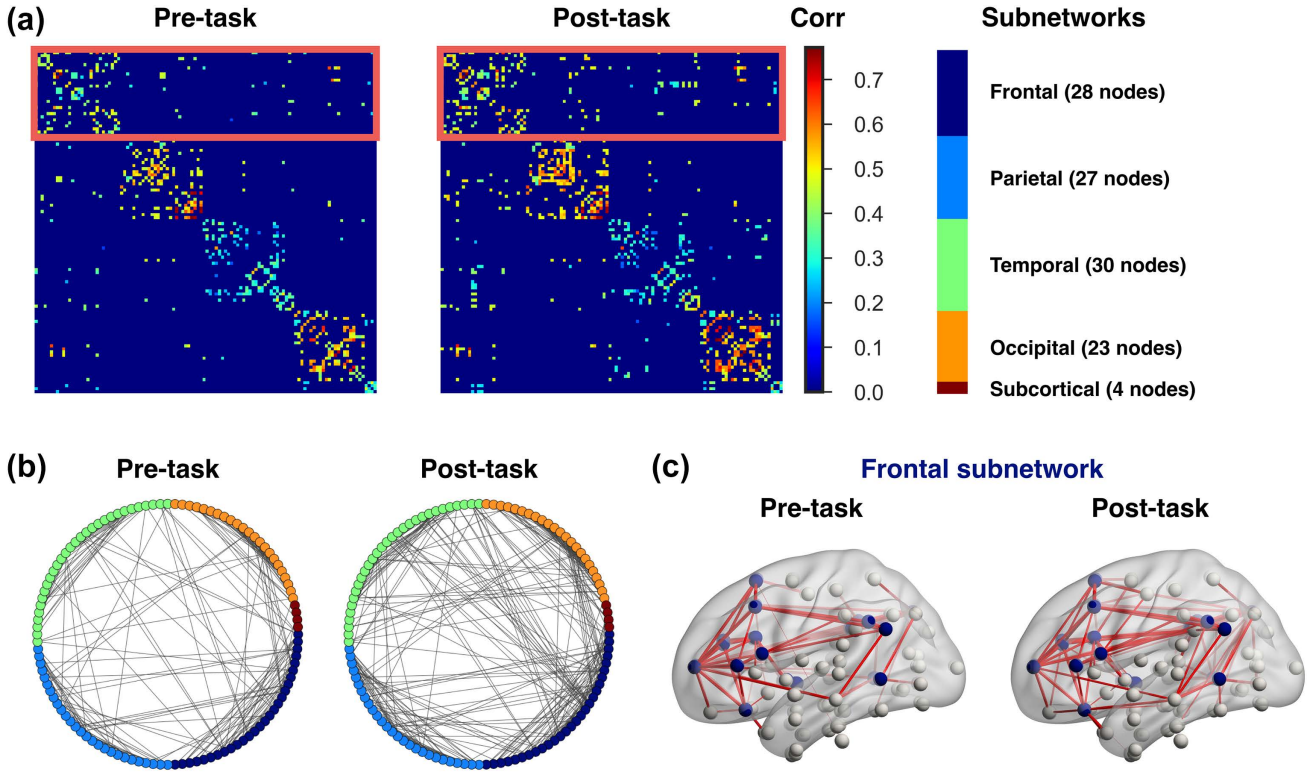

FIGURE 5 The averaged connection matrices across participants at pre- and posttask, rearranged with the representative community structure (a) and their circular representations (b). The color bar on the right in (a) indicates the identified subnetworks used to rearrange the connection matrices. The individual correlation matrices were averaged separately for pre- and posttask, and connection matrices were obtained with the same protocol as the individual connection matrices. Please note that these average graphs are only for demonstration purposes and were not used for the data analysis. As shown in (a), the OMST-based topological filtering produced topological graphs, in which weak connections were particularly maintained in the temporal subnetwork. The averaged networks appeared denser in the graph at posttask compared with the graph at pretask (a), particularly with intermodule connections (b). The frontal subnetwork and its connections with the other areas, which is highlighted with red rectangles overlaid on the connection matrices in (a), is depicted for pre- and posttask in (c). The intermodule connections in the frontal subnetwork increased at the posttask run

changes in cognitive performance and the discrimination between the pre- and posttask periods.

We first examined the behavioral performance and subjective feeling of the participants to ensure that performing the attention task actually induced mental fatigue. The behavioral analysis and the paper-based questionnaire for subjective scores of stress demonstrated that the selective attention task successfully induced significant TOT effects, which were manifested as increased RTs and decreased accuracies during the oddball task (Figure 4), consistent with previous studies on TOT effects (Lim et al., 2012; Lim et al., 2013; Lim et al., 2010), and decreased Engagement scores in the SSSQ (Matthews et al., 2013). Although cognitive proficiency through repetitive performance of the same task could also exert training effects on brain activity, the changes in behavioral performance observed in this study indicated an effect of mental fatigue rather than an effect of training. Second, the derived representative community structure of the functional network consisted of five subnetworks, that is, the frontal, parietal, temporal, occipital, and subcortical subnetworks (Figure 3), which were generally consistent with previous studies. Third, upon comparing the network characteristics of the whole network and the identified subnetworks at the pretask rest run (Rest1) with those at the posttask run (Rest2), only d_{FT} was selected with the feature selection and the subsequent logistic regression analysis showed a significant effect of d_{FT} in discriminating between Rest1 and Rest2 (Figure 6). Finally, four intermodule metrics, that is, d_{PT}, d_{TO}, L_{FT}, and L_{PO}, and three intramodule metrics, that is, d_F, L_P, and C_P, were selected out of twenty-seven features including three global network metrics (Table I), and the subsequent multivariate linear regression analysis showed significant powers of the all selected features for predicting individual cognitive decline measured with linear trends of changes in median RT during the task runs (Figures 7 and 8). As hypothesized, most of the associated changes in network topology with those in cognitive performance due to prolonged performance of the sustained attention task were found at the frontal and the parietal subnetworks, which are regarded to be flexible control-type networks, rather than static processing-type networks such as sensory-motor networks (Zanto & Gazzaley, 2013). Although we also examined the associations of changes in the network metrics with those in the subjective feelings of mental fatigue measured by the Engagement scale of the SSSQ questionnaire, no features were selected with the feature selection. As the SSSQ questionnaire was administered about 20–30 min after the posttask resting-state run, the associations may have been too weak to be detected.

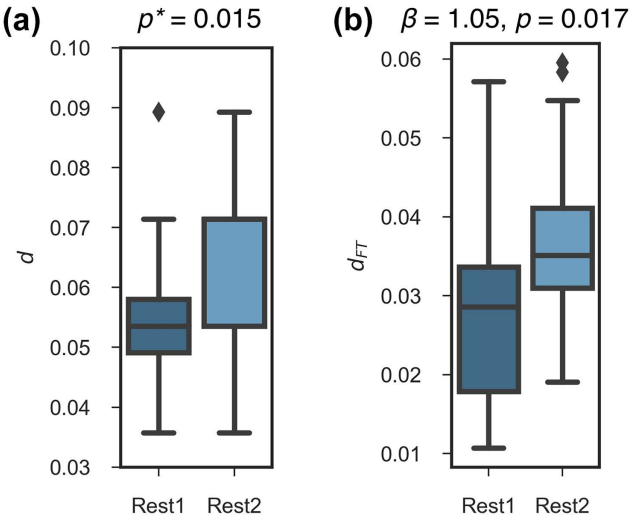

FIGURE 6 The density of the whole network d (a) and those in the intermodule density between the frontal and the temporal subnetworks d_{FT} (b) at Rest1 and Rest2. The significant difference in d were found with the non-parametric permutation test with 10,000 resamples, yielding an adjusted P value. Also, only d_{FT} was selected with the feature selection and the subsequent logistic regression analysis revealed a significant effect of d_{FT} in discriminating Rest1 and Rest2 [Color figure can be viewed at wileyonlinelibrary.com]

According to the partial regression plots, the intermodule connections between the parietal and the temporal subnetwork d_{PT} and those between the temporal and the occipital subnetworks d_{TO} became denser (Figure 7a, b), while the intermodule distance between the frontal and the temporal subnetworks L_{FT} got longer and those between the parietal and the occipital subnetworks L_{PO} got shorter for individuals with greater degree of cognitive decline (Figure 7c, d). Additionally, the frontal subnetwork was denser (Figure 8a) while the parietal subnetwork was less efficient in within-module communication (Figure 8b) and more clustered (Figure 8c) for individuals with less cognitive decline. The current analysis clearly demonstrated the changes of the network topology caused by the mental fatigue and suggests that network changes play a compensatory role for the declining cognitive ability due to fatigue. Further analysis using causal inference would provide additional information about causal relationships between the subnetworks. Moreover, a recovery from the mental fatigue may also have affected on the network topology, which would mingle with the compensatory process. The network changes should be correlated with some rates of recovery following the tasks.

Importantly, our results were obtained during resting-state scans, thus avoiding the potential confounding effects of worsening performance of the task itself, for example, changes in hemodynamic responses based on changes in response time (Domagalik, Beldzik, Oginska, Marek, & Fafrowicz, 2014). Additionally, the effects of mental fatigue were quite different among individuals, possibly depending on the degree of successful compensation for the declined cognitive ability. These findings suggest that we may be able to restrict the calculation of biomarkers for monitoring mental fatigue to the inter- and the intramodule network metrics of the fronto-parietal subnetworks, which showed significant predictive powers, allowing a reduction in the dimensionality of the feature space.

The TOT effects on the global characteristics of the resting-state functional network have been previously shown for resting-state fMRI networks (Breckel et al., 2013; Giessing et al., 2013; Sun et al., 2017) and for functional networks during task periods (Breckel et al., 2013). However, the network metrics for the whole network were not selected with the feature selection for the regression analysis for individual cognitive decline and the comparison between Rest1 and Rest2, suggesting that the inter- and the intramodule metrics had greater power for predicting the effect of mental fatigue on cognitive ability. As the changes in the cognitive performance are integrated consequence of complex changes in various cognitive functions, including declining attentional and visual processing or compensatory activity of the control-type subnetworks, the inter- and the intramodule metrics would provide more fine-grained information about alterations in the network topology due to mental fatigue.

While cost-integrated topological measures, which integrate the metric of interest with respect to a range of wiring cost or density, were used in the previous studies, a data-driven topological filtering scheme, which controlled density to maximize the cost-efficiency of the network, was employed in this study. It has been shown that the density level significantly influences network metrics (Ginestet, Nichols, Bullmore, & Simmons, 2011) and there is no reason to believe that the density level of a functional network is constant among individuals or even among different conditions within the same individual, supporting approaches that consider wiring costs, such as maximization of the cost-efficiency of the network (Bassett et al., 2009; Dimitriadis, Antonakakis, et al., 2017; Dimitriadis, Salis, et al., 2017). In this study, we found denser networks at posttask periods, which would generally result in higher efficiency of global and local information transfer. In other words, denser connections were necessary to retain the global efficiency of the network at posttask periods. Additionally, cost-integrated topological measures cannot be used with the community structure analysis as networks with different density levels produce different community structures with different number of communities. Thus, the optimization of cost-efficiency used in this study or other criteria would be mandatory to estimate actual networks.

The thresholding scheme used in this study has several advantages. First, as shown for EEG and fMRI functional networks (Dimitriadis, Salis, et al., 2017), the scheme based on OMSTs produced networks with greater normality of the distribution of shortest path lengths, as it allows non-strongest connections to be a part of the network. As such, the OMST-based scheme can retain subnetworks, which primarily consist of non-strongest connections, as shown for the temporal subnetwork in Figure 5. In this sense, this scheme is particularly compatible with community structure analysis. Second, as the scheme employs minimum spanning trees (MSTs), the resultant network has no isolated nodes, which distort network metrics and result in a fragmented community structure. More discussions about the OMSTs are found in APPENDIX A.

To study the modular organization of brain networks without ground truth, it is important to find a representative community structure of individual networks (Taya et al., 2016). However, individual networks can differ greatly among participants, and individual community structures can also vary as a result of individual differences in

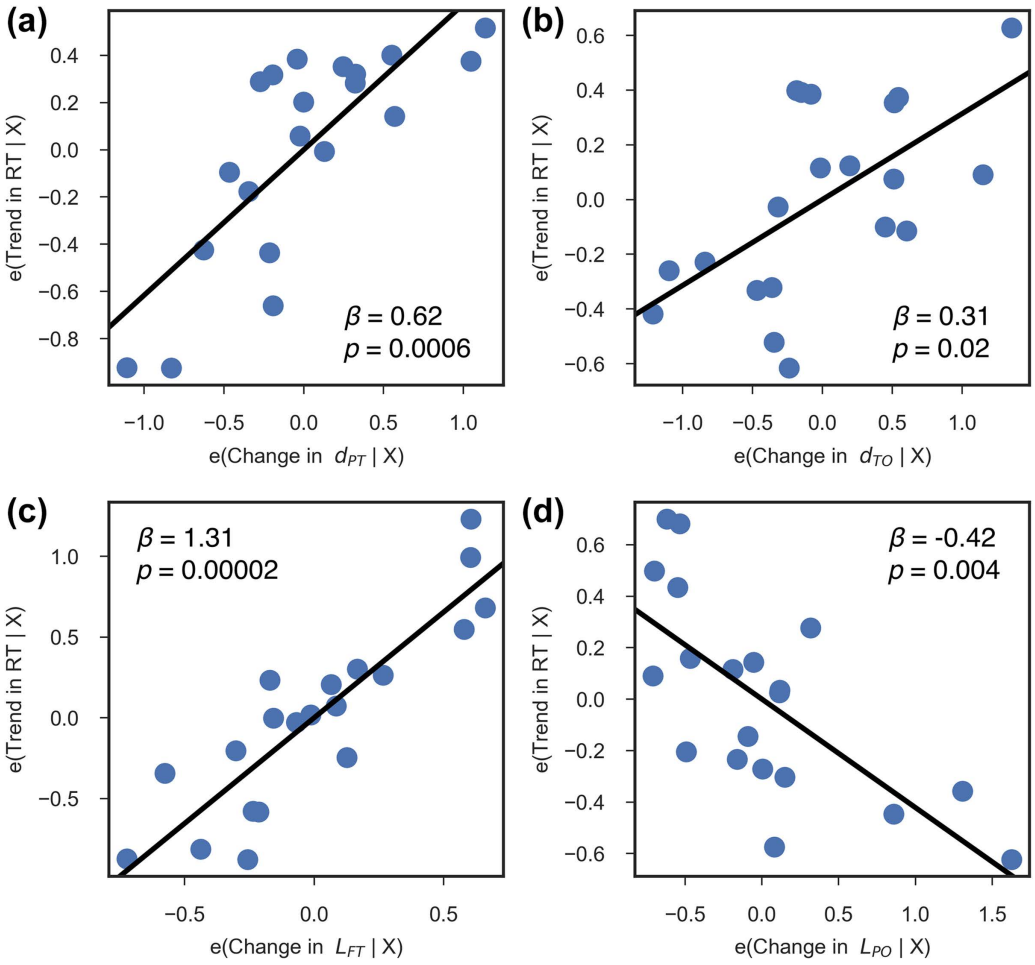

FIGURE 7 The partial regression plots showing the associations between the cognitive decline and the intermodule network metrics. Seven features including the four intermodule metrics and three intramodule metrics were selected out of twenty-seven features including network metrics for the whole network with the feature selection. The multivariate linear regression was performed to see whether the selected features had significant power in predicting individual linear trends in median RT during the task runs. While the intermodule density between the parietal and the temporal subnetworks d_{PT} (a), that between the temporal and the occipital subnetworks d_{TO} (b) and the intermodule characteristic path length between the frontal and the temporal subnetworks L_{FT} (c) showed positive effects, the intermodule characteristic path length between the parietal and the occipital subnetworks L_{PO} showed a negative effect (d) [Color figure can be viewed at wileyonlinelibrary.com]

connectivity patterns. Such between-subject variability can be attributed to genuine individual differences in connectivity or even artifacts associated with scanning or processing factors (Robinson, Atlas, & Wager, 2015). As such, consensus clustering was applied to the obtained individual community structure to obtain a representative community structure, which was used to calculate the network metrics of the subnetworks for each individual and each run. The resultant subnetworks identified with the community detection technique, which included frontal, parietal, temporal, occipital and subcortical subnetworks, were generally in agreement with those identified in previous studies of modular organization of functional brain networks (Cole et al., 2010; Crossley et al., 2013; He et al., 2009; Meunier, Achard, et al., 2009; Meunier, Lambiotte, et al., 2009; Power et al., 2011; Yeo et al., 2011).

Community structure analysis can provide additional information about mesoscale network organization of the brain and can serve as a bridge between univariate approaches and graph theoretical network metrics of the large-scale network. By decomposing networks into subnetworks, we can investigate not only the roles of brain regions but also the roles of subnetworks consisting of brain regions dedicated to common cognitive functions and their relationships. Our results suggest that the topological nature of the particular inter- and the intramodule connections has differing flexibility to compensate for cognitive decline due to mental fatigue, which cannot directly be examined with univariate approaches or network metrics that quantify the local or global characteristics of the network topology of the entire network.

There remain several issues to be addressed in the future. First, a comparison with task-related activation could provide further valuable insight regarding the alterations due to mental fatigue in modular organization and the topological roles of subnetworks induced by the performing the task. Second, a direct comparison with changes in EEG power associated with mental fatigue or with the topological properties of functional networks derived from EEG signals acquired simultaneously with fMRI data would provide further insight into EEG biomarkers for mental fatigue. Third, studies on dynamics of networks

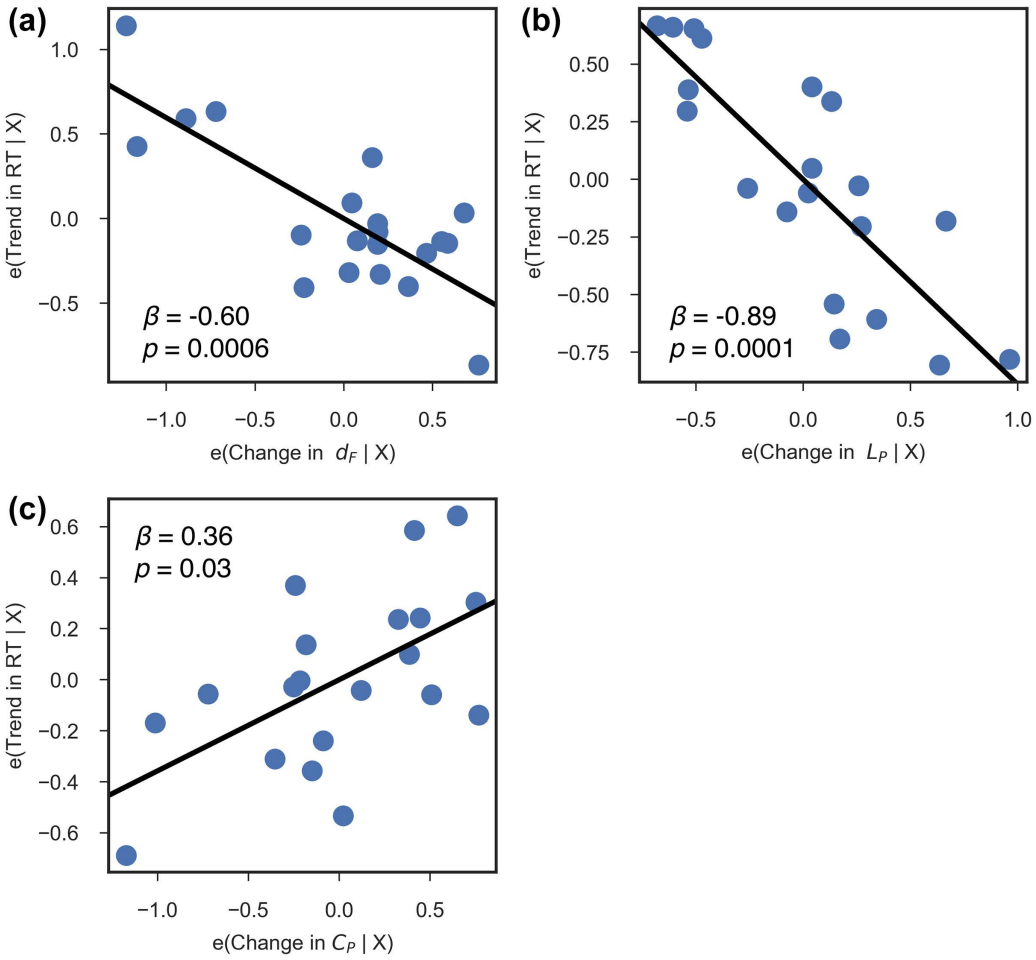

FIGURE 8 The partial regression plots showing the associations between the cognitive decline and the intramodule network metrics selected with the feature selection. The multivariate linear regression analysis revealed that, while the intramodule density of the frontal subnetwork d_F (a) and the intramodule characteristic path length of the parietal subnetwork L_P (b) showed negative effects, the intramodule clustering coefficient of the parietal subnetwork C_P (c) showed a positive effect [Color figure can be viewed at wileyonlinelibrary.com]

would demonstrate dynamical reconfiguration of subnetwork topology due to mental fatigue and its recovery. Finally, community structure analysis on directed networks would provide further useful information about the mutual relationships between subnetworks regarding cognitive decline due to mental fatigue and causal roles of the subnetworks in compensation for the declining cognitive ability.

5 | CONCLUSION

In this study, we investigated the short-term effects induced by prolonged performance of a sustained attention task on the modular organization of the brain intrinsic functional network. We developed the inter- and the intramodule network metrics to quantify the topological characteristics of connections between and within subnetworks. Regression models with the feature selection were used to examine which metrics were effective in predicting individual cognitive decline, as well as in discriminating the pre- and the posttask runs. We found that the density of intermodule connections between the frontal and temporal subnetworks had a greater power in predicting the pre- and the posttask runs than other metrics including those for the whole networks. Also, the changes in seven inter- or intramodule metrics, mostly at the fronto-parietal subnetworks, showed significant predictive power of individual cognitive decline measured with increases in reaction time. Interestingly, most of the metrics showing predictive powers were found at the flexible control-type fronto-parietal networks, supporting our hypothesis that control-type networks exhibit flexible alterations in network topology to compensate for cognitive decline due to mental fatigue. Though still in its infancy, community structure analysis on human brain functional networks will provide further insight into the neural mechanisms behind cognitive states including mental fatigue.

ACKNOWLEDGMENTS

The authors declare that they have no competing interests. They thank the National University of Singapore for supporting the grants Cognitive Engineering under WBS R-719-001-102–232 and Prof. Thakor Startup under R-719-000-200-133. SD was supported by a MRC grant MR/K004360/1 (Behavioural and Neurophysiological Effects of Schizophrenia Risk Genes: A Multi-locus, Pathway Based Approach) as well as a MARIE-CURIE COFUND EU-UK Research

Fellowship. The authors also acknowledge Dr. Rahul Rathakrishnan for his support in consultancy.

ORCID

Stavros I. Dimitriadis http://orcid.org/0000-0002-0000-5392
Anastasios Bezerianos http://orcid.org/0000-0002-8199-6000

REFERENCES

Alexander-Bloch, A., Lambiotte, R., Roberts, B., Giedd, J., Gogtay, N., & Bullmore, E. (2012). The discovery of population differences in network community structure: new methods and applications to brain functional networks in schizophrenia. *Neuroimage*, *59*(4), 3889–3900.

Barwick, F., Arnett, P., & Slobounov, S. (2012). EEG correlates of fatigue during administration of a neuropsychological test battery. *Clinical Neurophysiology*, *123*(2), 278–284.

Bassett, D. S., Bullmore, E. T., Meyer-Lindenberg, A., Apud, J. A., Weinberger, D. R., & Coppola, R. (2009). Cognitive fitness of cost-efficient brain functional networks. *Proceedings of the National Academy of Sciences*, *106*(28), 11747–11752.

Bassett, D. S., Porter, M. A., Wymbs, N. F., Grafton, S. T., Carlson, J. M., & Mucha, P. J. (2013). Robust detection of dynamic community structure in networks. *Chaos: An Interdisciplinary Journal of Nonlinear Science*, *23*(1), 013142.

Bassett, D. S., Wymbs, N. F., Porter, M. A., Mucha, P. J., Carlson, J. M., & Grafton, S. T. (2011). Dynamic reconfiguration of human brain networks during learning. *Proceedings of the National Academy of Sciences United States of America*, *108*(18), 7641–7646.

Blondel, V. D., Guillaume, J.-L., Lambiotte, R., & Lefebvre, E. (2008). Fast unfolding of communities in large networks. *Journal of Statistical Mechanics: Theory and Experiment*, *2008*(10), P10008.

Bonnefond, A., Doignon-Camus, N., Touzalin-Chretien, P., & Dufour, A. (2010). Vigilance and intrinsic maintenance of alert state: An ERP study. *Behavioural Brain Research*, *211*(2), 185–190.

Brainard, D. H. (1997). The Psychophysics Toolbox. *Spatial Vision*, *10*(4), 433–436.

Breckel, T. P., Thiel, C. M., Bullmore, E. T., Zalesky, A., Patel, A. X., & Giessing, C. (2013). Long-term effects of attentional performance on functional brain network topology. *PLoS One*, *8*(9), e74125.

Bressler, S. L., & Menon, V. (2010). Large-scale brain networks in cognition: emerging methods and principles. *Trends in Cognitive Sciences*, *14*(6), 277–290.

Bullmore, E., & Sporns, O. (2009). Complex brain networks: graph theoretical analysis of structural and functional systems. *Nature Reviews Neuroscience*, *10*(3), 186–198.

Cole, D. M., Smith, S. M., & Beckmann, C. F. (2010). Advances and pitfalls in the analysis and interpretation of resting-state FMRI data. *Frontiers in Systems Neuroscience*, *4*, 8.

Cole, M. W., Reynolds, J. R., Power, J. D., Repovs, G., Anticevic, A., & Braver, T. S. (2013). Multi-task connectivity reveals flexible hubs for adaptive task control. *Nature Neuroscience*, *16*(9), 1348–1355.

Craig, A., Tran, Y., Wijesuriya, N., & Nguyen, H. (2012). Regional brain wave activity changes associated with fatigue. *Psychophysiology*, *49*(4), 574–582.

Crossley, N. A., Mechelli, A., Vertes, P. E., Winton-Brown, T. T., Patel, A. X., Ginestet, C. E., … Bullmore, E. T. (2013). Cognitive relevance of the community structure of the human brain functional coactivation network. *Proceedings of the National Academy of Sciences United States of America*, *110*(28), 11583–11588.

Davies, D. R., & Parasuraman, R. (1982). *The psychology of vigilance*. Academic Pr.

Dimitriadis, S. I., Antonakakis, M., Simos, P., Fletcher, J. M., & Papanicolaou, A. C. (2017). Data-driven Topological Filtering based on Orthogonal Minimal Spanning Trees: Application to Multi-Group MEG Resting-State Connectivity. *Brain Connect*, *7*, 661–670.

Dimitriadis, S. I., Salis, C., Tarnanas, I., & Linden, D. E. (2017). Topological Filtering of Dynamic Functional Brain Networks Unfolds Informative Chronnectomics: A Novel Data-Driven Thresholding Scheme Based on Orthogonal Minimal Spanning Trees (OMSTs). *Frontiers in Neuroinformatics*, *11*,

Domagalik, A., Beldzik, E., Oginska, H., Marek, T., & Fafrowicz, M. (2014). Inconvenient correlation - RT-BOLD relationship for homogeneous and fast reactions. *Neuroscience*, *278*, 211–221.

Fortunato, S. (2010). Community detection in graphs. *Physics Reports*, *486*(3–5), 75–174.

Fuertinger, S., & Simonyan, K. (2016). Stability of Network Communities as a Function of Task Complexity. *J Cogn Neurosci*, *28*, 2030–2043.

Giessing, C., Thiel, C. M., Alexander-Bloch, A. F., Patel, A. X., & Bullmore, E. T. (2013). Human brain functional network changes associated with enhanced and impaired attentional task performance. *Journal of Neuroscience*, *33*(14), 5903–5914.

Ginestet, C. E., Nichols, T. E., Bullmore, E. T., & Simmons, A. (2011). Brain network analysis: separating cost from topology using cost-integration. *PLoS One*, *6*(7), e21570.

Godwin, D., Barry, R. L., & Marois, R. (2015). Breakdown of the brain's functional network modularity with awareness. *Proceedings of the National Academy of Sciences of the United States of America*, *112*(12), 3799–3804.

Han, K., Mac Donald, C. L., Johnson, A. M., Barnes, Y., Wierzechowski, L., Zonies, D., … Brody, D. L. (2014). Disrupted modular organization of resting-state cortical functional connectivity in U.S. military personnel following concussive 'mild' blast-related traumatic brain injury. *Neuroimage*, *84*, 76–96.

Hastie, T., Tibshirani, R., & Friedman, J. (2009). *The elements of statistical learning*, the second edition. New York: Springer.

He, Y., & Evans, A. (2010). Graph theoretical modeling of brain connectivity. *Current Opinion in Neurology*, *23*(4), 341–350.

He, Y., Wang, J., Wang, L., Chen, Z. J., Yan, C., Yang, H., … Evans, A. C. (2009). Uncovering intrinsic modular organization of spontaneous brain activity in humans. *PLoS One*, *4*(4), e5226.

Helton, W. S. (Validation of a short stress state questionnaire) (2004). SAGE Publications. p 1238–1242.

Jenkinson, M., Beckmann, C. F., Behrens, T. E., Woolrich, M. W., & Smith, S. M. (2012). Fsl. *Neuroimage*, *62*(2), 782–790.

Kar, S., Routray, A., & Nayak, B. P. (2011). Functional network changes associated with sleep deprivation and fatigue during simulated driving: validation using blood biomarkers. *Clinical Neurophysiology*, *122*(5), 966–974.

Kennedy, D. N., Lange, N., Makris, N., Bates, J., Meyer, J., & Caviness, V. S. Jr. (1998). Gyri of the human neocortex: an MRI-based analysis of volume and variance. *Cerebral Cortex*, *8*(4), 372–384.

Lancichinetti, A., & Fortunato, S. (2012). Consensus clustering in complex networks. *Scientific Reports*, *2*(1),

Ledoit, O., & Wolf, M. (2004). A well-conditioned estimator for large-dimensional covariance matrices. *Journal of Multivariate Analysis*, *88*(2), 365–411.

Lim, J., Ebstein, R., Tse, C. Y., Monakhov, M., Lai, P. S., Dinges, D. F., & Kwok, K. (2012). Dopaminergic polymorphisms associated with time-on-task declines and fatigue in the Psychomotor Vigilance Test. *PLoS One*, *7*(3), e33767.

Lim, J., Quevenco, F. C., & Kwok, K. (2013). EEG alpha activity is associated with individual differences in post-break improvement. *Neuroimage*, *76*, 81–89.

Lim, J., Wu, W. C., Wang, J., Detre, J. A., Dinges, D. F., & Rao, H. (2010). Imaging brain fatigue from sustained mental workload: an ASL perfusion study of the time-on-task effect. *Neuroimage*, *49*(4), 3426–3435.

Lindsay, R. W., Percival, D. B., & Rothrock, D. (1996). The discrete wavelet transform and the scale analysis of the surface properties of sea ice. *IEEE Transactions on Geoscience and Remote Sensing*, *34*(3), 771–787.

Mackworth, N. H. (1948). The Breakdown of Vigilance during Prolonged Visual Search. *The Quarterly Journal of Experimental Psychology*, *1*(1), 6–21.

Makris, N., Meyer, J. W., Bates, J. F., Yeterian, E. H., Kennedy, D. N., & Caviness, V. S. (1999). MRI-Based topographic parcellation of human cerebral white matter and nuclei II. Rationale and applications with systematics of cerebral connectivity. *Neuroimage*, *9*(1), 18–45.

Matthews, G., Szalma, J., Panganiban, A. R., Neubauer, C., & Warm, J. S. (2013). Profiling task stress with the Dundee Stress State Questionnaire. Psychology of stress: New research. p 49–90.

Meunier, D., Achard, S., Morcom, A., & Bullmore, E. (2009). Age-related changes in modular organization of human brain functional networks. *Neuroimage*, *44*(3), 715–723.

Meunier, D., Lambiotte, R., & Bullmore, E. T. (2010). Modular and hierarchically modular organization of brain networks. *Frontiers in Neuroscience*, *4*, 200.

Meunier, D., Lambiotte, R., Fornito, A., Ersche, K. D., & Bullmore, E. T. (2009). Hierarchical modularity in human brain functional networks. *Frontiers in Neuroinformatics*, *3*, 37.

Murphy, K., Birn, R. M., Handwerker, D. A., Jones, T. B., & Bandettini, P. A. (2009). The impact of global signal regression on resting state correlations: are anti-correlated networks introduced?. *Neuroimage*, *44*(3), 893–905.

Newman, M. E., & Girvan, M. (2004). Finding and evaluating community structure in networks. *Physical Review. E, Statistical, Nonlinear, and Soft Matter Physics*, *69*(2 Pt 2), 026113.

Newman, M. E. J. (2012). Communities, modules and large-scale structure in networks. *Nature Physics*, *8*(1), 25–31.

North, B. V., Curtis, D., & Sham, P. C. (2002). A note on the calculation of empirical P values from Monte Carlo procedures. *American Journal of Human Genetics*, *71*(2), 439–441.

Pelli, D. G. (1997). The VideoToolbox software for visual psychophysics: Transforming numbers into movies. *Spatial Vision*, *10*(4), 437–442.

Power, J. D., Barnes, K. A., Snyder, A. Z., Schlaggar, B. L., & Petersen, S. E. (2012). Spurious but systematic correlations in functional connectivity MRI networks arise from subject motion. *Neuroimage*, *59*(3), 2142–2154.

Power, J. D., Cohen, A. L., Nelson, S. M., Wig, G. S., Barnes, K. A., Church, J. A., … Petersen, S. E. (2011). Functional network organization of the human brain. *Neuron*, *72*(4), 665–678.

Radicchi, F., Castellano, C., Cecconi, F., Loreto, V., & Parisi, D. (2004). Defining and identifying communities in networks. *Proceedings of the National Academy of Sciences of the United States of America*, *101*(9), 2658–2663.

Robinson, L. F., Atlas, L. Y., & Wager, T. D. (2015). Dynamic functional connectivity using state-based dynamic community structure: method and application to opioid analgesia. *Neuroimage*, *108*, 274–291.

Rubinov, M., & Sporns, O. (2010). Complex network measures of brain connectivity: uses and interpretations. *Neuroimage*, *52*(3), 1059–1069.

See, J. E., Howe, S. R., Warm, J. S., & Dember, W. N. (1995). Meta-analysis of the sensitivity decrement in vigilance. *Psychological Bulletin*, *117*(2), 230–249.

Sham, P. C., & Purcell, S. M. (2014). Statistical power and significance testing in large-scale genetic studies. *Nature Reviews Genetics*, *15*(5), 335–346.

Sporns, O. (2013). The human connectome: origins and challenges. *NeuroImage*, *80*, 53–61.

Sporns, O., & Betzel, R. F. (2016). Modular brain networks. *Annual Review of Psychology*, *67*, 613.

Stevens, A. A., Tappon, S. C., Garg, A., & Fair, D. A. (2012). Functional brain network modularity captures inter- and intra-individual variation in working memory capacity. *PLoS One*, *7*(1), e30468.

Sun, Y., Lim, J., Dai, Z., Wong, K., Taya, F., Chen, Y., … Bezerianos, A. (2017). The effects of a mid-task break on the brain connectome in healthy participants: A resting-state functional MRI study. *Neuroimage*, *152*, 19–30.

Sun, Y., Lim, J., Kwok, K., & Bezerianos, A. (2014). Functional cortical connectivity analysis of mental fatigue unmasks hemispheric asymmetry and changes in small-world networks. *Brain and Cognition*, *85*, 220–230.

Sun, Y., Yin, Q., Fang, R., Yan, X., Wang, Y., Bezerianos, A., … Sun, J. (2014). Disrupted functional brain connectivity and its association to structural connectivity in amnestic mild cognitive impairment and Alzheimer's disease. *PLoS One*, *9*(5), e96505.

Tanaka, M., Shigihara, Y., Ishii, A., Funakura, M., Kanai, E., & Watanabe, Y. (2012). Effect of mental fatigue on the central nervous system: an electroencephalography study. *Behavioral and Brain Functions*, *8*(1), 48.

Taya, F., de Souza, J., Thakor, N. V., & Bezerianos, A. (2016). Comparison method for community detection on brain networks from neuroimaging data. *Applied Network Science*, *1*(1), 8.

Tong, Y., & Frederick, B. D. (2014). Studying the spatial distribution of physiological effects on BOLD signals using ultrafast fMRI. *Frontiers in Human Neuroscience*, *8*,

Trejo, L. J., Kubitz, K., Rosipal, R., Kochavi, R. L., & Montgomery, L. D. (2015). EEG-based estimation and classification of mental fatigue. *Psychology*, *06*(05), 572.

van den Heuvel, M. P., de Lange, S. C., Zalesky, A., Seguin, C., Yeo, B. T., & Schmidt, R. (2017). Proportional thresholding in resting-state fMRI functional connectivity networks and consequences for patient-control connectome studies: Issues and recommendations. *Neuroimage*, *152*, 437–449.

Wascher, E., Rasch, B., Sanger, J., Hoffmann, S., Schneider, D., Rinkenauer, G., … Gutberlet, I. (2014). Frontal theta activity reflects distinct aspects of mental fatigue. *Biological Psychology*, *96*, 57–65.

Watts, D. J., & Strogatz, S. H. (1998). Collective dynamics of 'small-world' networks. *Nature*, *393*(6684), 440–442.

Whitcher, B., Guttorp, P., & Percival, D. B. (2000). Wavelet analysis of covariance with application to atmospheric time series. *Journal of Geophysical Research: Atmospheres*, *105*(D11), 14941–14962.

Yeo, B. T., Krienen, F. M., Sepulcre, J., Sabuncu, M. R., Lashkari, D., Hollinshead, M., … Buckner, R. L. (2011). The organization of the human cerebral cortex estimated by intrinsic functional connectivity. *Journal of Neurophysiology*, *106*(3), 1125–1165.

Zanto, T. P., & Gazzaley, A. (2013). Fronto-parietal network: flexible hub of cognitive control. *Trends in Cognitive Sciences*, *17*(12), 602–603.

Zhang, Z., Telesford, Q. K., Giusti, C., Lim, K. O., & Bassett, D. S. (2016). Choosing wavelet methods, filters, and lengths for functional brain network construction. *PLoS One*, *11*(6), e0157243.

SUPPORTING INFORMATION

Additional Supporting Information may be found online in the supporting information tab for this article.

How to cite this article: Taya F, Dimitriadis SI, Dragomir A, et al. Fronto-Parietal Subnetworks Flexibility Compensates For Cognitive Decline Due To Mental Fatigue. *Hum Brain Mapp*. 2018;39:3528–3545. https://doi.org/10.1002/hbm.24192

APPENDIX A: TOPOLOGICAL FILTERING WITH OMSTS

In this study, the thresholding scheme proposed by Dimitriadis and colleagues (Dimitriadis, Antonakakis, et al., 2017; Dimitriadis, Salis, et al., 2017) was employed, which is an iterative approach that optimizes the global cost efficiency of the graph (Bassett et al., 2009) by accumulating OMSTs. The OMSTs make up the orthogonal set of the minimum spanning trees (MST), which is a subgraph of the graph consisting of edges connecting all of the original graph, with no cycles and with the minimum total wiring costs. The OMSTs are obtained by iteratively finding an MST for the rest of the graph after removing the edges of the MST at the previous step. Compared to other popular thresholding schemes based on the strength of connections, for example, the selection of a certain proportion of the strongest connections, the OMST-based approach extracts connections without differentiating weak from strong connections while preserving the advantage of MSTs by retaining no isolated nodes. Therefore, we believe that the OMST-based thresholding scheme is compatible with the community structure analysis. Actually, this thresholding scheme was shown to outperform other well-known thresholding schemes in terms of the recognition accuracy of individuals based on EEG data and the reproducibility of

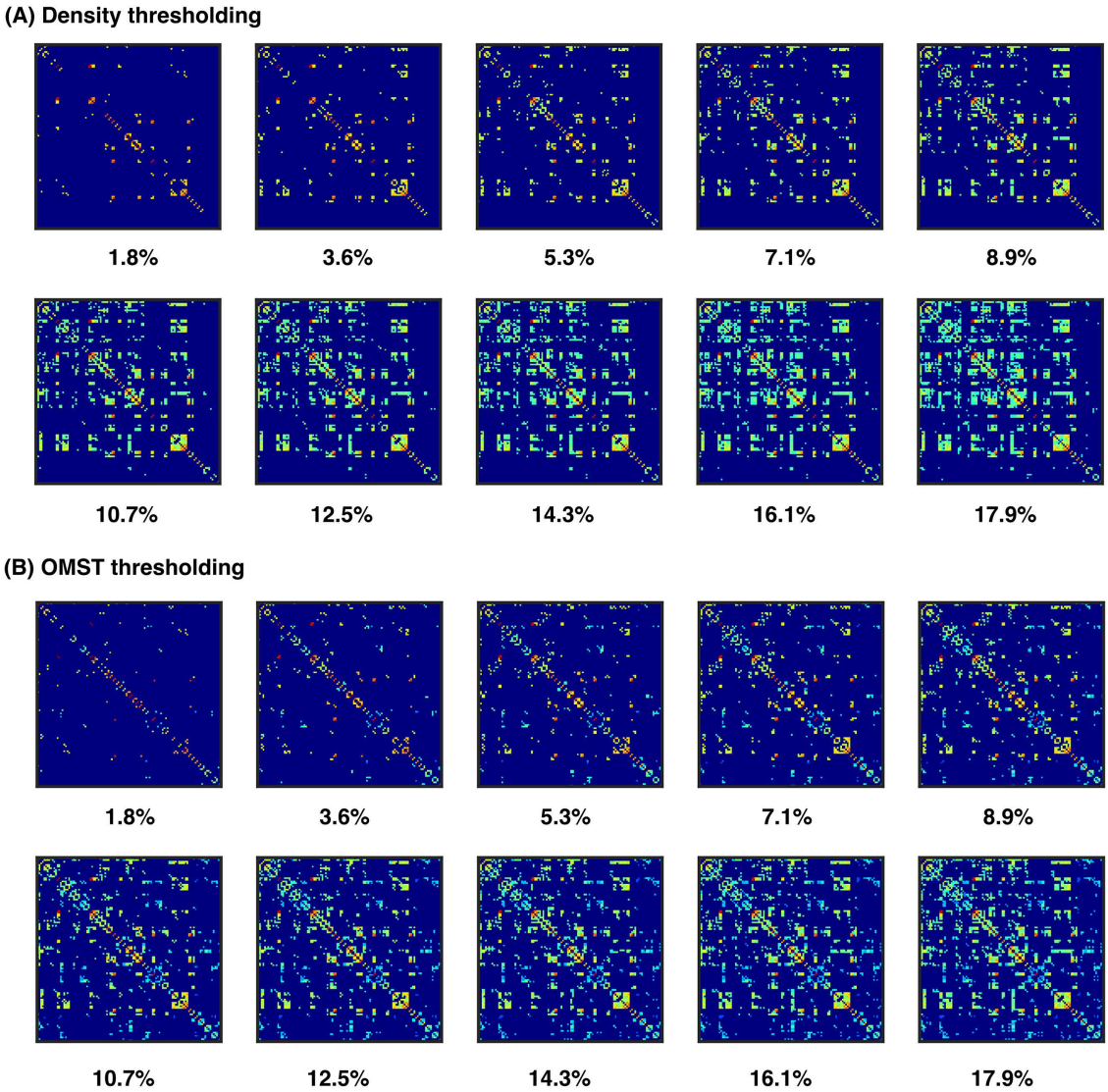

FIGURE A1 The averaged connection matrices across participants at Rest1. The matrices were thresholded with the density thresholding scheme (a) and the OMST-based thresholding scheme (b). While the density thresholding does not extract weak connections at the bottom and the right side of the matrices, which would produce disconnected nodes and fragmented community structures, the OMST thresholding extracts connections from a wide range of the matrix without differentiating weak ones. As the density level increases, the connection matrices produced by both thresholding schemes converged.

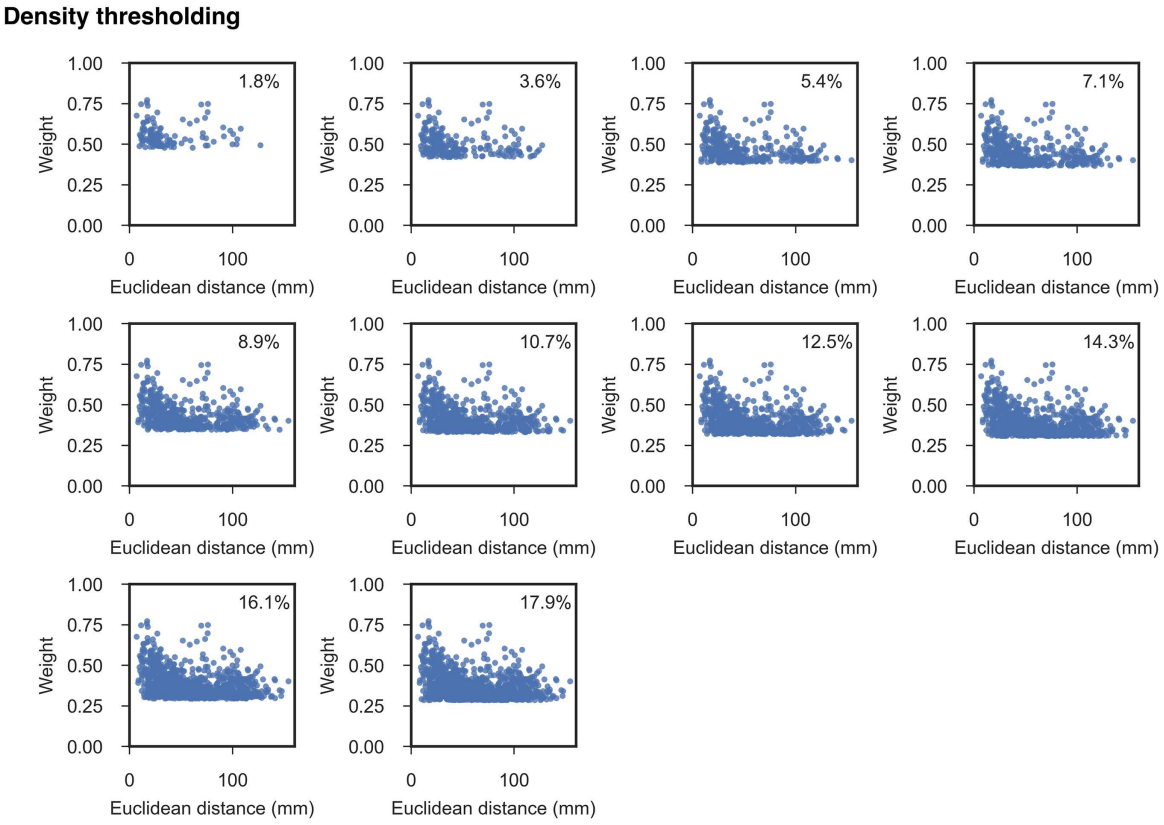

FIGURE A2 The relationships between the Euclidean distance and weights of connections extracted with the density thresholding scheme. The extracted connections were biased toward the upper part of the figures although the distances of the connections were widely distributed. [Color figure can be viewed at wileyonlinelibrary.com]

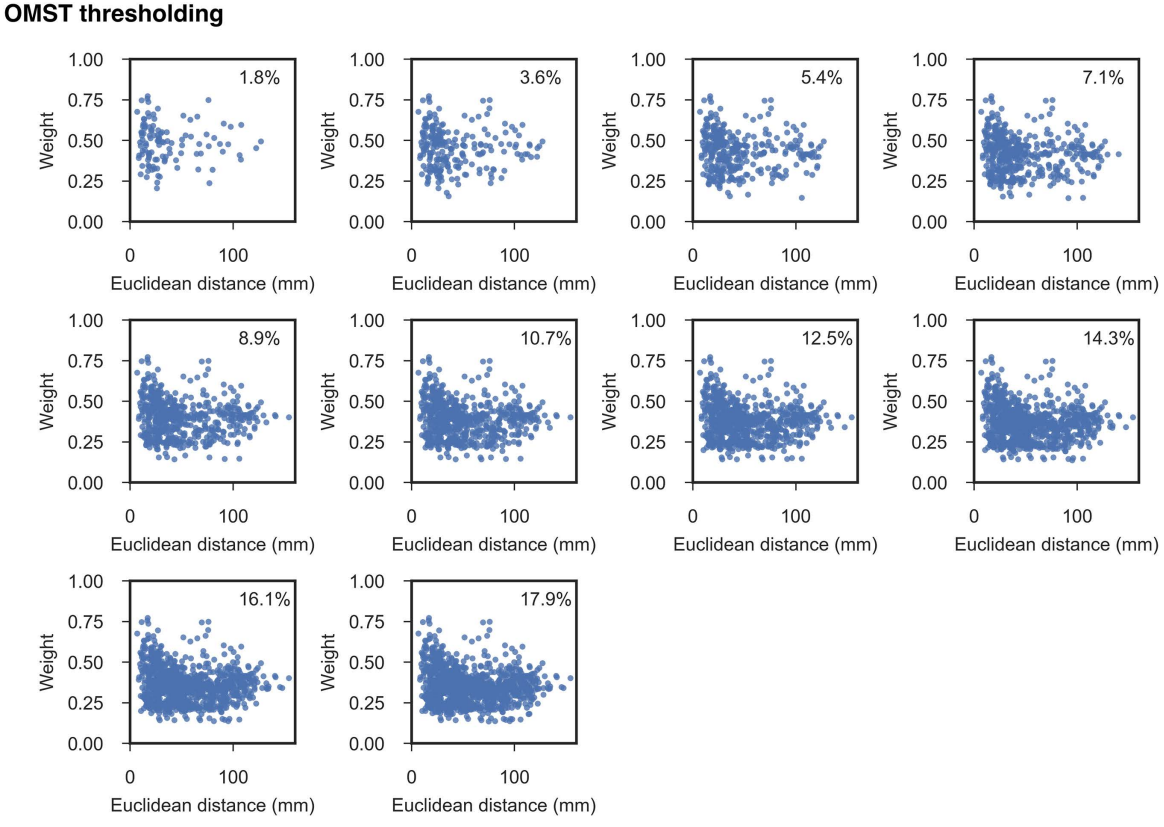

FIGURE A3 The relationships between the Euclidean distance and weights of connections extracted with the OMST thresholding scheme. The connections were extracted from a wide range of both distances and weights [Color figure can be viewed at wileyonlinelibrary.com]

network metrics measured via intra-class correlation (ICC) for a single-subject fMRI data scanned 100 times (Dimitriadis, Salis, et al., 2017). Also, the study using the OMST thresholding scheme successfully classified resting-state MEG networks derived from four groups of participants, that is, healthy adults, adults with mild traumatic brain injury, typically developing children and reading-disabled children, while the functional networks thresholded with the conventional MST-based scheme showed low accuracy (Dimitriadis, Antonakakis, et al., 2017).

To show advantages of the thresholding scheme based on OMSTs over that based on the strength of connections, we applied both scheme to the averaged connection matrix among participants at Rest1. We first obtained accumulated OMSTs for the connection matrix up to ten OMSTs (Figure A1b). Then, the proportional thresholding scheme on the strength of connections (van den Heuvel et al., 2017) was applied at the density levels of the obtained ten networks with OMSTs, that is, 1.8% to 17.9%. As shown in Figure 1, while the OMST-based thresholding extracted connections in wide portions of the matrix, the density thresholding did not extract weak connections particularly in some specific portions of the matrices, resulting in disconnected nodes or a fragmented community structure. As such, when we see the relationships between the weights and the Euclidean distances of the extracted connections, the connections extracted with the density thresholding, which simply cut off weakest connections, were biased toward the upper part of the figures, discarding most of the connections in the lower part of the figures, although the distances of the extracted connections were widely distributed (Figure 2). On the other hand, the OMST thresholding extracted weak connections as well as strong ones from a wide range of distances (Figure 3). As the correlation-based connection strengths are weaker for signals with lower signal-to-noise ratio, spatial distribution of noises in the signals has significant impacts on spatial distributions of noises in estimated weights. As physiological noises in BOLD signals are not uniformly distributed in the brain (Tong & Frederick, 2014), noises in connection strengths should not be uniformly distributed as well, violating the basic assumptions behind the thresholding schemes based on connectivity strengths such as the density thresholding. Taken together, the OMST-based thresholding scheme extracts connections from wide range of brain areas without differentiating weak connections and produces networks with no isolated nodes, all of which would be great advantages for the community structure analysis as well as network analysis on large-scale networks.

APPENDIX B: MODULARITY

Partitioning of the network nodes into modules was completed by maximizing the modularity index Q, which represents the density of links inside modules compared to links between modules. The modularity index Q is defined as

$$Q=\frac{1}{2m}\sum_{i,j}\left[W_{ij}-\gamma\frac{k_i k_j}{2m}\right]\delta(c_i,c_j)$$

where W_{ij} is the weight of the edge between node i and node j, γ is the spatial resolution parameter, k_i is the sum of the weights of the edges linking to node i, c_i is the community to which node i belongs, the δ-function $\delta(u,v)$ is 1 if $u = v$ and 0 otherwise, and $m=\sum_{ij}W_{ij}$. For networks with strong community structures, the modularity index typically falls in the range of 0.3 to 0.7 (Newman & Girvan, 2004). Here, the spatial resolution parameter, γ, is a hyper-parameter, which must be defined a priori. Higher γ detects more communities, while lower γ detects larger communities.